European Journal of Chemistry

View Journal Online
View Article Online

DFT structural analysis of salen-type Fe(II) complexes and their docking behavior toward laccase

Takahiro Kawaguchi [1], Daisuke Nakane [1], Takashiro Akitsu [1,*], Abul Monsur Showkot Hossain [2], and Qobilova Malika Qudratovna [2]

[1] *Department of Chemistry, Faculty of Science, Tokyo University of Science, Tokyo, 162-8601, Japan*
[2] *Faculty of Chemistry, Termez State University, Barkamol Avlod Str. 43, Termez 190111, Uzbekistan*

* *Corresponding author at: Department of Chemistry, Faculty of Science, Tokyo University of Science, Tokyo, 162-8601, Japan.*
e-mail: akitsu2@rs.tus.ac.jp (T. Akitsu).

RESEARCH ARTICLE

10.5155/eurjchem.17.1.69-78.2776

Received: 1 January 2026
Received in revised form: 16 February 2026
Accepted: 3 March 2026
Published online: 31 March 2026
Printed: 31 March 2026

KEYWORDS

Iron
Laccase
UV-vis spectroscopy
Infrared spectroscopy
Circular dichroism spectroscopy
Density functional theory calculations

ABSTRACT

In this study, we report the molecular design of chiral Schiff base Fe(II) complexes with and without azobenzene moieties, their structural optimization using density functional theory (DFT), and their interaction with laccase. The UV-vis and polarized IR spectra of the complexes were simulated using time-dependent density functional theory (TD-DFT), demonstrating that irradiation with linearly polarized ultraviolet light can induce specific supramolecular arrangements within the chiral laccase matrix. This study highlights the importance of computational chemistry in predicting the structure of metal complexes, protein binding behavior, and light absorption properties, thereby enabling the evaluation of expected functionalities prior to experimental investigation.

Cite this: *Eur. J. Chem.* **2026**, *17(1)*, 69-78 **Journal website**: www.eurjchem.com

1. Introduction

Laccase [1-3] is used as an enzyme at the cathode of biofuel cells [4-7], where oxygen is reduced to water via a four-electron reaction. To improve the energy production efficiency of biofuel cells, it is necessary to improve electron transfer from the electrode to the enzyme (especially the electron-receiving T1 site [1] in the case of laccase).

To overcome this limitation, a mediator is usually placed between the cathode and the enzyme. Nanoparticle mediators have spatial advantages because they are incorporated into protein molecules; however, they exhibit a low current density. On the contrary, metal complex mediators [6] have the advantage of high current densities; however, their molecular size and shape render them incompatible with protein molecules and generally limit electron transfer over long distances.

Therefore, there remains a pressing need for metal complexes with well-defined spatial architectures, as well as for convenient strategies to achieve precise spatial control and organization [8-10]. In addition to conventional applications using photoisomerization [11], our laboratory has extensively investigated the incorporation of organic/inorganic hybrid materials consisting of functional metal complexes and azobenzene moieties [12,13] into polymer films, where optical anisotropy (i.e. anisotropic molecular orientation) can be induced by linearly polarized UV light via the Weigert effect [14,15]. These systems were developed to prepare bidentate chiral Schiff base complexes [12,13], salen-type chiral Schiff base complexes [16,17], nonchiral complexes [18,19], complexes with azobenzene fractions [20,21], and materials without azobenzene fractions (where the dipole moment of the metal complex is large) [21,22].

Synthetic polymer films, as well as protein films [22,23], have been used as templates, and the binding of metal–protein complexes has been discussed [22,24]. Furthermore, recent reports have revealed the existence of UV-induced circularly polarized supramolecular chirality or photoinduced helical supramolecular arrangements [18,25]. Therefore, polarization-induced molecular orientation may be a promising method to control the spatial orientation of metal-protein complexes and their binding to protein surfaces [26].

In this study, we treated Fe(II) salen-type Schiff-based chiral complexes (Figure 1) with and without azobenzene moieties. We discuss the results of structural optimization using density functional theory (DFT) and the docking results with laccase for these Fe(II) complexes.

ISSN 2153-2249 (Print) / ISSN 2153-2257 (Online)
https://dx.doi.org/10.5155/eurjchem.17.1.69-78.2776

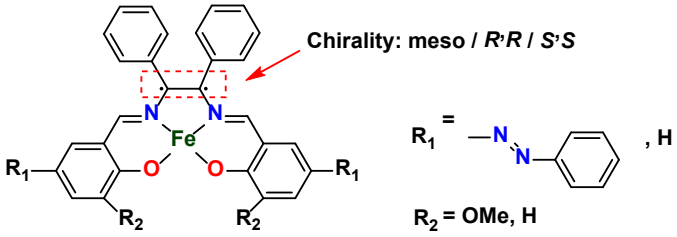

Figure 1. Structures of Fe(II) complexes with and without azobenzene moieties.

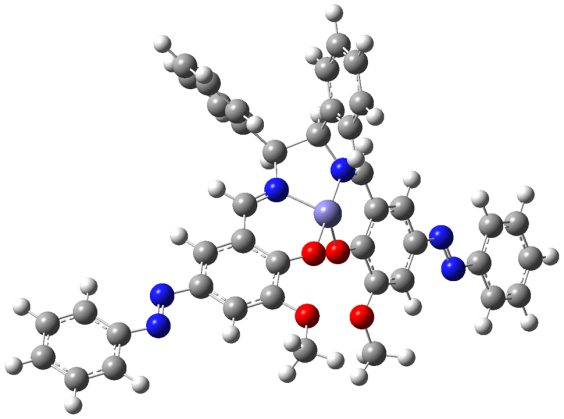

Figure 2. Structural optimization of azo-containing meso-*o*-vaniline-Fe(II) complex. The colors of the atoms were as follows: white (H), gray (C), blue (N), red (O), and the central atom purple (Fe).

The motivation of this study was to use computational chemistry to verify whether expected functions could be realized with respect to the structure of the metal complex, protein binding, and light absorption before conducting actual experiments.

2. Experimental

2.1. Instrumentation

Quantum chemical calculations were performed using Gaussian 09W (Revision D.01, Gaussian, Inc.) [27] on the chiral salen-type Schiff base Fe(II) complexes synthesized with and without azobenzene moieties. The optimized structures of the salen-type Fe(II) complexes depend on the central metal ion, its oxidation state, and the ligand environment. Using the obtained ground-state optimized structures, we performed docking calculations for the laccase and Fe(II) complex using GOLD [28]. Furthermore, docking simulations were performed using the 1GYC crystal structure [3] obtained from the PDB using the GOLD program [28] at the CCDC. A Windows PC was used for all calculations.

2.2. Theoretical studies

For molecular modeling, the initial input structures of the salen-type Fe(II) complexes were constructed based on experiments using condensation of salicylaldehyde, *o*-vanillin, and 1,2-diphenylethylenediamine (meso, *R*,*R*, and *S*,*S*) to form the corresponding Schiff base ligands, which subsequently coordinated to the metal center. Geometry optimization was performed using the B3LYP functional. The LANL2D2 basis set was used for Fe atoms and the 6-31+G(d) basis set was used for H, C, N, and O atoms. Furthermore, using the optimized structures, energy analyses of the initial (HOMO) and late (LUMO) orbitals were performed at the same theoretical level (B3LYP/LANL2DZ for Fe and 6-31+G(d) for H/C/N/O) to compare the electronic states. Based on a recent report [29], the search region was set to a pocket around the T1 site with a search radius of 15-19 Å. The calculations were performed using the B3LYP functional method, which has been widely used in many studies because of its excellent computational efficiency and accuracy [30,31], and the LANL2DZ basis set [30,32], which effectively incorporates relativistic effects to accurately analyze the heavy elements in the metal ion moiety of the complex.

To confirm that the optimized structure represents the true energy minimum, vibrational frequency calculations were performed simultaneously with structure optimization using the same calculation parameters. During the optimization process, molecular electrostatic potential (MEP) maps and HOMO and LUMO surfaces were constructed to investigate the chemical reactivity and biological potential of the metal complexes. Analysis of the energy gap between the HOMO and LUMO regions provides insight into their electronic properties [30]. Furthermore, the geometries of the synthesized compounds (complexes) were optimized using DFT, providing a reliable foundation for the construction of accurate docking models. Prior to the docking simulations, crystallographic water molecules were removed from the protein structure. These procedures enhanced the accuracy and reliability of the docking analysis, thereby enabling more robust and consistent docking simulations [30].

3. Results and Discussion

3.1. DFT

Geometry optimization (Figures 2-5), energy analyzes of the initial (HOMO) and late orbitals (LUMO) (Figures 6-9), DFT-simulated UV-Vis and IR spectra (Figures 10-13), as well as docking simulations of PDB 1GYC using the GOLD program [28] at the CCDC (Figures 14 and 15) are indicated below.

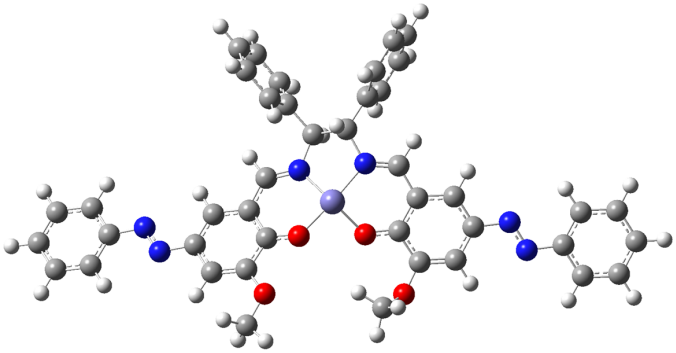

Figure 3. Structural optimization of azo-containing *R,R-o*-vaniline-Fe(II) complex. The colors of the atoms were as follows: white (H), gray (C), blue (N), red (O), and the central atom purple (Fe).

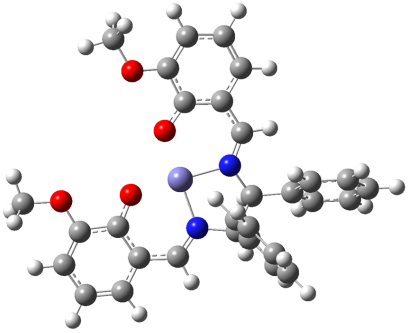

Figure 4. Structural optimization of azo- free meso-*o*-vaniline-Fe(II) complex. The colors of the atoms were as follows: white (H), gray (C), blue (N), red (O), and the central atom purple (Fe).

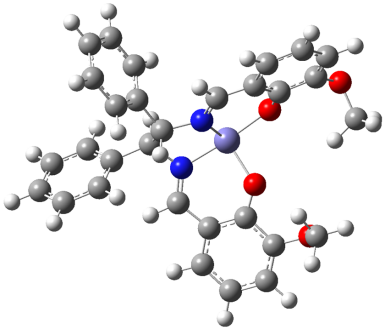

Figure 5. Structural optimization of azo-free *R,R-o*-vaniline-Fe(II) complex. The colors of the atoms were as follows: white (H), gray (C), blue (N), red (O), and the central atom purple (Fe).

Frontier molecular orbital (FMO) analyzes were performed to clarify the electronic properties and reactivity of compounds such as salen complexes. Salen complexes, which are typically Schiff base ligands coordinated to a central metal ion, have been widely studied for applications in catalysis, molecular recognition, and materials science. FMO analyzes, including HOMO and LUMO, were performed to determine the chemical stability of the molecules [30]. These analyses revealed the ability of the molecules to act as electron donors or acceptors, providing valuable insight into their reactivity and distinctive structural features. The HOMO-LUMO energy gap (ΔE) plays an important role in the kinetic stability, chemical reactivity, and biological activity of molecules. A smaller ΔE increases the efficiency of intramolecular charge transfer along conjugated pathways and facilitates electron transfer from electron-donating groups to electron-accepting groups within the molecule [30]. Compounds with narrower ΔE generally exhibit higher chemical reactivity and biological activity, but lower kinetic stability. Conversely, compounds with wider energy gaps tend to exhibit lower reactivity and biological activity, but higher kinetic stability [30]. The ΔE values of these Fe(II) complexes were measured to be approximately 2.5-3.5 eV (Figures 6-9).

Frontier molecular orbital analysis of the optimized complex revealed important features of its electronic structure. HOMO was primarily located in the metal center and the phenolate moiety, whereas LUMO was distributed throughout the π-conjugated ligand framework. The calculated HOMO-LUMO energy gap for the Ni(II) complex is 3.112 eV, which is comparable to the values reported for the Fe(II) and Ni(II) complexes with similar ligand environments. The slightly smaller energy gap compared to that of the Ni(II) analog suggests higher chemical reactivity and lower kinetic stability. In contrast, similarity to the Fe(II) complex indicates similar electronic properties. These findings suggest that the electronic structure of this complex is strongly influenced by the ligand field and π-conjugation [33].

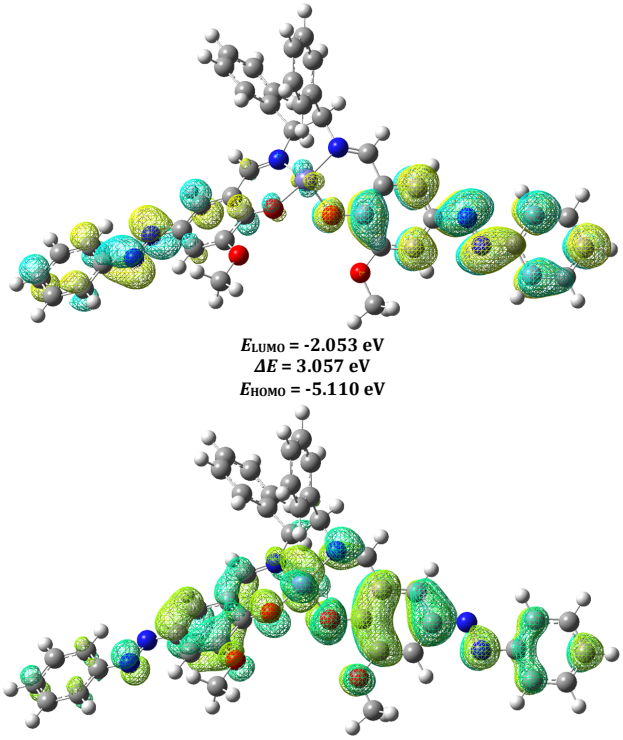

Figure 6. HOMO/LUMO of an azo-containing meso-*o*-vaniline-Fe(II) complex.

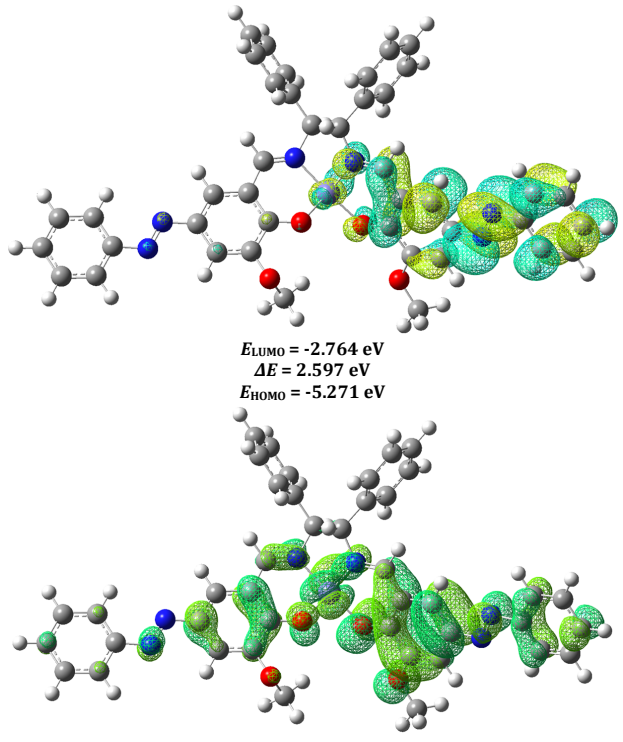

Figure 7. HOMO/LUMO of an azo-containing *R,R-o*-vaniline-Fe(II) complex.

To estimate the solution structures of the Fe(II) complexes, geometry optimizations were performed using time-dependent density functional theory (TD-DFT). On the basis of the optimized structures, simulated IR and UV-Vis spectra were generated (Figures 10-13). The simulated spectra adequately reproduced the main features of the experimental data, consistent with previously reported procedures [16]. The simulated infrared spectra peaks for each Fe(II) ion appeared at approximately 3000, 1500, 1000, and 500 cm^{-1}. Vibrational bands were identified at approximately 3391 cm^{-1} for ν(OH) and approximately 1610 cm^{-1} for ν(CH=N–, azomethine) [30]. A sharp characteristic band corresponding to the ν(CH = N) band of the coordinated Schiff base ligand was identified at approximately 1610 cm^{-1} [30].

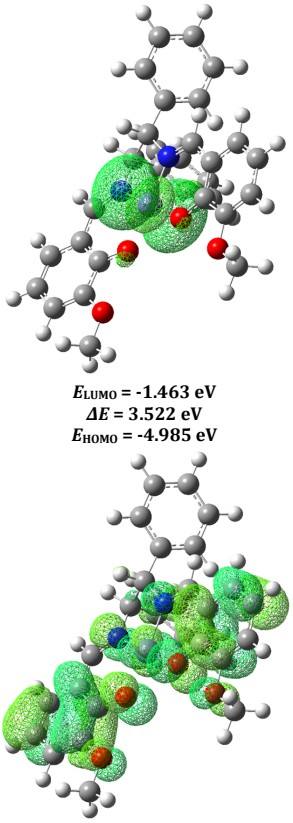

Figure 8. HOMO/LUMO of an azo-free meso-*o*-vaniline-Fe(II) complex.

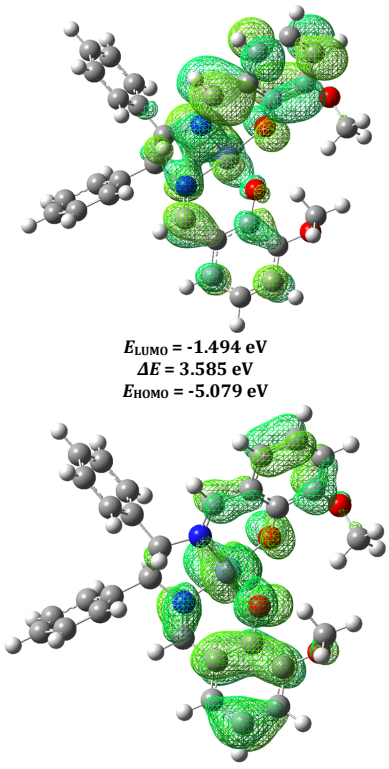

Figure 9. HOMO/LUMO of an azo-free *R,R-o*-vaniline-Fe(II) complex.

Absorption bands due to aromatic groups appeared in all complexes in the range of approximately 2928–2980 cm^{-1}, corresponding to stretching vibrations [30]. Absorption bands were observed in the range of about 3400-3000 cm^{-1} and about 634-658 cm^{-1}, attributed to hydrogen bonding involving non-coordinated and lattice water molecules.

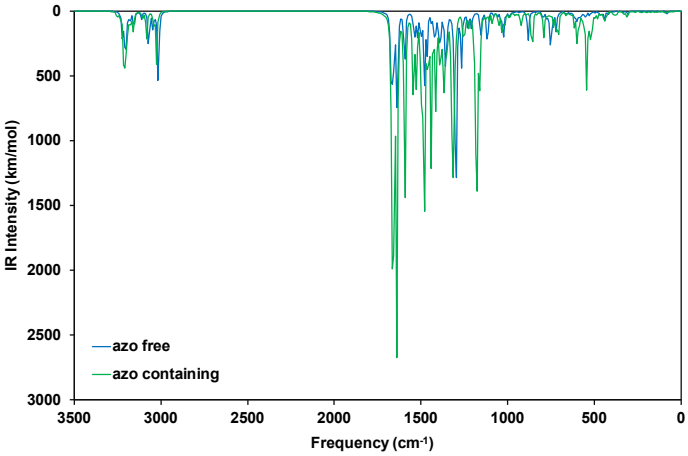

Figure 10. Infrared spectra of the azo-containing and azo-free meso-*o*-vaniline-Fe(II) complex.

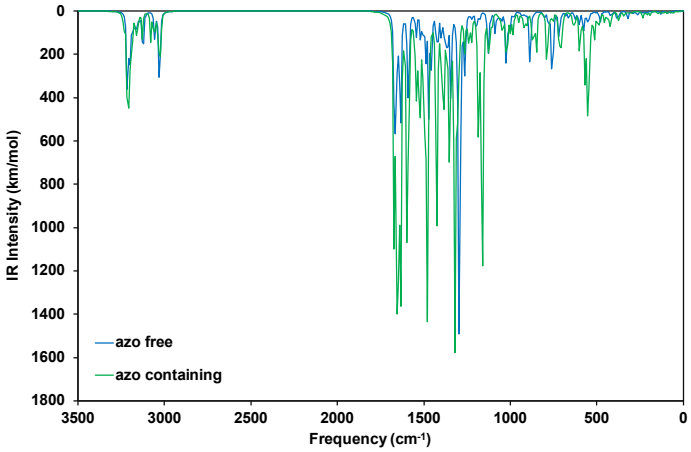

Figure 11. Infrared spectra of the azo-containing and azo-free *R,R*-*o*-vaniline-Fe(II) complex.

Furthermore, two new absorption bands appeared in the IR spectrum of the complex; one attributable to ν(M-O) in the range of about 547-556 cm^{-1} [30].

CD spectra of the simulated ions using TD-DFT confirmed that linearly polarized UV irradiation induces specific supramolecular arrangements in the chiral laccase matrix and that the circular polarization response differs between the *R,R*- and S,S-enantiomers. The main absorption band (419 nm, from HOMO-1(189) to LUMO+3(191)) is also correlated with the experimentally observed increase in current density. The HOMO/LUMO distribution varied depending on the presence and absence of azo groups, with the azo-binding system stabilized near T1. The CD spectrum of the azo-containing Fe(II)-meso-*o*-vanillin complex was not analyzed in further detail because a reliable circular polarization signal could not be obtained under current computational conditions.

The calculated IR spectra (Figures 10 and 11) of the Fe(II) complexes (both with and without azo groups) showed characteristic absorption bands corresponding to C=N and phenolic C–O stretching vibrations. The C=C stretching vibration appears around 1500 cm^{-1}. Additionally, the C=N stretching vibration appears around 1640 cm^{-1} and is shifted compared to the free ligand, suggesting coordination via the imine nitrogen atom. A phenolic C-O stretching vibration was observed between 1000 and 1300 cm^{-1}, suggesting deprotonation and coordination through the oxygen atom. The calculated IR spectra showed bands corresponding to ligand vibrations in the 1000-1300 cm^{-1} region, although individual assignments were complicated by vibrational mode coupling. Similar IR spectral features have been reported for related Zn(II) Schiff base complexes, in which coordination occurs via the imine nitrogen and phenolic oxygen atoms. This agreement with reported trends supports the proposed coordination mode for this complex [34].

The calculated UV-Vis spectra (Figure 12) of the Fe(II) complex show intense absorption bands in the 200–300 nm region, which can be assigned to ligand-centered π → π* transitions and metal-to-ligand charge transfer (MLCT) transitions. Compared with the reported Ni(II) salen-type complexes, which typically exhibit absorption bands around 245 nm attributed to *d-d* and LMCT transitions, the present Fe(II) complex shows (red-shifted/blue-shifted) features [33]. Furthermore, previous studies have shown that the UV-Vis spectra of Co(II), Zn(II), Ni(II), and Mn(II) complexes exhibit strong absorption bands in the 300-500 nm region. Compared with these Co(II), Zn(II), Ni(II), and Mn(II) complexes, the present Fe(II) complex shows slightly shifted absorption bands, which may be attributed to differences in d-electron configuration and ligand field strength [33].

The calculated CD spectra (Figure 13) exhibit characteristic Cotton effects corresponding to the chiral coordination environment around the Fe(II) center. These Cotton effect arises from the asymmetric ligand field generated by the chiral arrangement (*e.g.*, *S,S* configuration) of the Schiff base ligands, which creates a distinct chiral environment around the metal ion.

Table 1. Goldscore of the azo-containing meso-*o*-vaniline-Fe(II) complex.

Fitness	External HBond weighted	External Vdw weighted	Internal torsion weighted	Internal Vdw weighted
0	3.9204	-81.7794	-11.2044	-148.4519
0	9.6952	-78.6192	-18.1134	-67.4596
0	15.8422	-77.1869	-15.5685	-97.3477
0	4.1453	-39.3579	-11.9539	-241.3694
0	4.1137	-70.0727	-14.2245	-106.1535
0	1.7289	-72.9590	-9.6715	-80.0025
0	1.7289	-66.1080	-13.0600	-88.9897
-588.3286	0.1658	-579.3802	-8.5255	-2.4786
0	9.2627	-72.7619	-11.8065	-22.7276
0	10.2606	-59.0027	-18.3663	-111.1212

Table 2. Goldscore of the azo-containing *R,R*-*o*-vaniline-Fe(II) complex.

Fitness	External HBond weighted	External Vdw weighted	Internal torsion weighted	Internal Vdw weighted
0	0	-68.1665	-12.7801	-44.9824
0	7.2498	-52.0478	-12.4736	-85.0352
-1056.9372	0.3707	-1043.0452	-10.1402	-16.9840
0	0	-65.2523	-8.9471	-49.5390
0	2.2482	-75.7469	-15.8369	-72.0884
0	12.2677	-83.4247	-9.4388	-34.0074
0	5.5214	-50.7599	-11.1923	-80.1842
0	16.2184	-64.6390	-9.9759	-96.9922
-1001.1189	1.7901	-993.0854	-8.9249	-13.4677
-986.1426	0	-964.0376	-7.4771	-27.1969

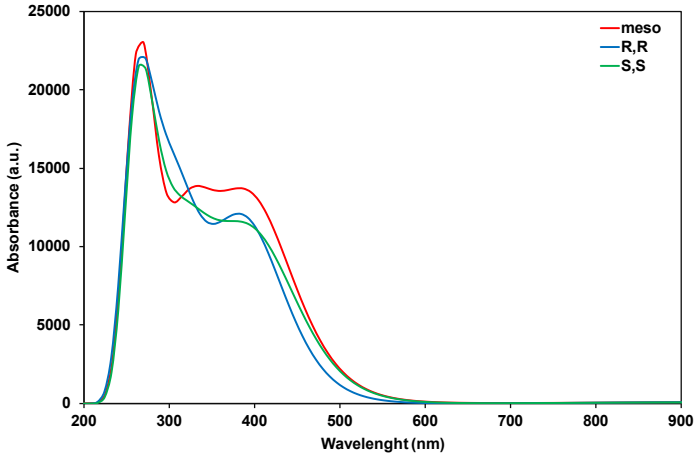

Figure 12. UV-vis spectra of azo-free -*o*-vaniline-Fe(II) complex (meso, *R,R*, and *S,S*).

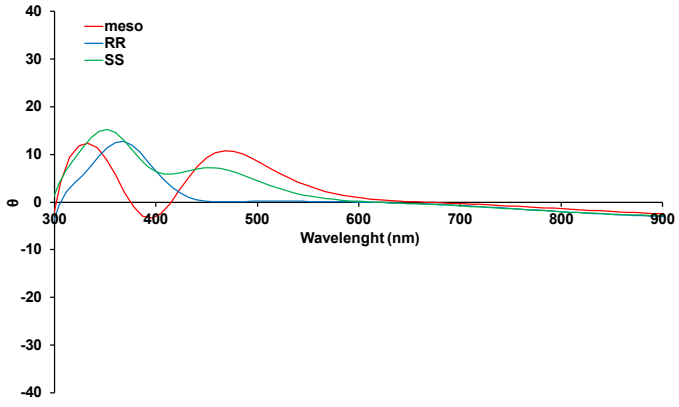

Figure 13. CD spectra of the azo-free -*o*-vaniline-Fe(II) complex (meso/*R,R*/*S,S*).

In previous studies, similar CD spectral features have been reported for related Co(II), Zn(II), Ni(II), and Mn(II) Schiff base complexes, indicating that the chiral ligand arrangement significantly influences the electronic transitions. This agreement with reported trends suggests that the optimized structure reasonably reproduces the stereochemical and chiral environment of the complex.

3.2. GOLD docking simulation

Using Fe(II) complexes and molecular docking simulations, the potential biological activities of the compounds were explored, and their binding affinity and interactions with target biomolecules were elucidated (Tables 1-4, Figures 14-17) [30].

Table 3. Goldscore of the azo-free meso-*o*-vaniline-Fe(II) complex.

Fitness	External HBond weighted	External Vdw weighted	Internal torsion weighted	Internal Vdw weighted
-502.2433	0	-485.7224	-11.2047	-9.2003
-659.1095	0	-637.8439	-11.1305	-14.0193
-544.6001	0	-514.9437	-9.0740	-24.4666
-645.9620	0.3157	-625.5825	-12.3702	-11.9591
-717.9764	1.929	-699.0083	-10.4480	-14.0619
-803.1063	0	-786.1431	-11.6950	-8.8810
-833.7972	0.7594	-800.7869	-10.1742	-27.2085
-1204.6324	10.0824	-1176.7585	-11.8723	-29.6969
0	14.6178	-88.9944	-19.1826	-15.9132
-827.7444	15	-810.8282	-22.9022	-12.6269

Table 4. Goldscore of the azo-containing *R,R-o*-vaniline-Fe(II) complex.

Fitness	External HBond weighted	External Vdw weighted	Internal torsion weighted	Internal Vdw weighted
0	1.4077	-950.8532	-2.6788	-39.9198
-1132.0041	13.5607	-1139.9534	-2.0459	-21.9035
-836.3586	1.1181	0774.9293	-2.3778	-78.5076
-763.8683	13.5105	-728.5566	-2.4755	-64.6847
-917.9970	1.1468	-851.7061	-2.2121	-83.5635
-1299.5886	3.2509	-1293.0650	-2.8144	-25.2981
-879.2548	1.9445	-816.1708	-2.4546	-80.9120
-1225.7357	4.8970	-1164.6404	-2.5441	-81.6534
0	13.3780	-106.8642	-1.1478	-40.0252
-1678.2578	4.0842	-1647.6200	-4.4298	-48.4974

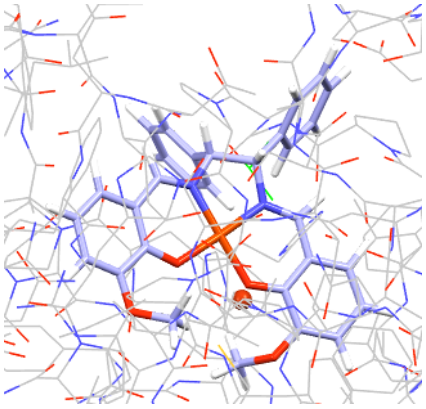

Figure 14. Structures of Fe(II) complexes without azobenzene moieties (meso).

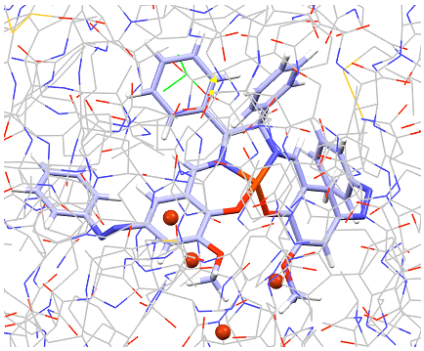

Figure 15. Structures of Fe(II) complexes with azobenzene moieties (meso).

Computational approaches predict the preferred binding mode and identify key residues and functional groups involved in interactions [30]. Furthermore, by analyzing docking scores and visualizing molecular poses, promising candidate compounds with favorable binding profiles were identified [30]. These compounds can be further optimized to clarify their efficacy and mechanistically analyze their binding to their targets [30]. Molecular docking simulations were performed to study the compounds. This advanced computational method not only confirms the observed biological activity, but also reveals important interactions in the binding mechanism [30].

The molecular docking results showed that the azo-containing Fe(II) complex exhibited a higher GOLD score than the non-azo-containing Fe(II) complex, indicating good binding affinity to laccase. This high score suggested that the complex could form stable interactions within the active site, including hydrogen bonding and hydrophobic interactions. Such interactions are expected to contribute significantly to the overall stability of the ligand–protein complex.

Hydrophobic and hydrogen-bonding interactions between Fe(II) complexes and the protein play an important role in stabilizing the enzyme-inhibitor complex and maintaining the integrity of the active site, as evidenced by the strong binding affinity of these compounds toward the enzyme active site [30].

In particular, these interactions are reinforced by an extensive network of strong hydrogen bonds and hydrophobic

contacts, suggesting the potential of these compounds as effective enzyme inhibitors [30].

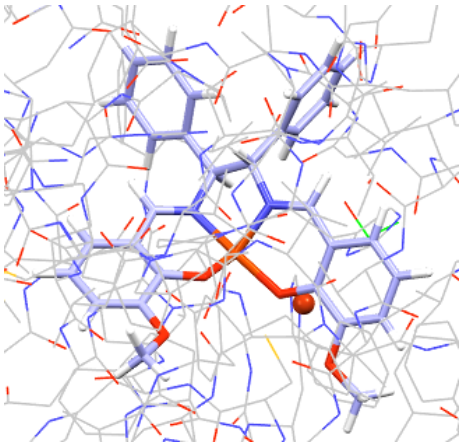

Figure 16. Structures of Fe(II) complexes without azobenzene moieties (*R,R*).

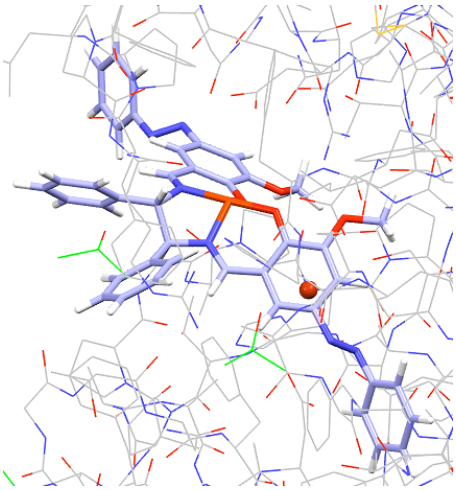

Figure 17. Structures of Fe(II) complexes with azobenzene moieties (*R,R*).

Molecular docking results showed that the azo-containing Fe(II) complex exhibited a higher GOLD score than the azo-free Fe(II) complex, indicating stronger binding affinity to the target protein. Previous docking studies (including those with Cu(II) complexes) have demonstrated that higher GOLD scores indicate stronger binding interactions and improved stability of the ligand-protein complex. This high score suggests that the azo-containing complex formed stable interactions within the active site, including hydrogen bonds and hydrophobic contacts. These interactions are expected to contribute significantly to the stability of the ligand-protein complex, thus supporting the proposed binding mode [35].

4. Conclusions

In summary, we have investigated chiral Fe(II) salen-type Schiff base complexes that potentially exhibit the Weigert effect (anisotropic molecular orientation) upon irradiation with polarized ultraviolet (UV) light, with or without azobenzene molecules. We then performed structural optimization using DFT and discussed the results of co-binding with laccase. These complexes bind to laccase in a surface pocket near the T1 site. Computational results showed that irradiation of this Fe(II)-laccase complex with polarized UV light significantly increased the current density by controlling the molecular orientation of the laccase. We believe that this photocontrolled intermediate represents a promising new molecular design strategy for applications in biofuel cell cathodes. Further research on this method and similar materials is currently underway.

Disclosure statement

Conflicts of interest: The authors declare that they have no conflict of interest.
Ethical approval: All ethical guidelines have been adhered to.
Sample availability: Samples of the compounds are available from the author.

CRediT authorship contribution statement

Conceptualization: Takashiro Akitsu; Methodology: Takashiro Akitsu; Investigation: Takahiro Kawaguchi; Writing—Original Draft: Takahiro Kawaguchi, Abul Monsur Showkot Hossain, Qobilova Malika Qudratovna; Review and Editing: Abul Monsur Showkot Hossain, Qobilova Malika Qudratovna, Daisuke Nakane, Takashiro Akitsu; Project Administration: Takashiro Akitsu.

ORCID and Email

Takahiro Kawaguchi
1325702@ed.tus.ac.jp
https://orcid.org/0009-0008-3380-8088
Daisuke Nakane
a29776@rs.tus.ac.jp
https://orcid.org/0000-0001-9566-0674
Takashiro Akitsu
akitsu2@rs.tus.ac.jp
https://orcid.org/0000-0003-4410-4912
Abul Monsur Showkot Hossain
monsur_12@yahoo.com
https://orcid.org/0000-0002-2339-3391
Qobilova Malika Qudratovna
malikaqobilova353@gmail.com
https://orcid.org/0009-0003-5705-3293

References

[1]. Augustine, A. J.; Kragh, M. E.; Sarangi, R.; Fujii, S.; Liboiron, B. D.; Stoj, C. S.; Kosman, D. J.; Hodgson, K. O.; Hedman, B.; Solomon, E. I. Spectroscopic Studies of Perturbed T1 Cu Sites in the Multicopper Oxidases *Saccharomyces cerevisiae* Fet3p and *Rhus vernicifera* Laccase: Allosteric Coupling between the T1 and Trinuclear Cu Sites. *Biochemistry* **2008**, *47* (7), 2036–2045.
[2]. Farver, O.; Wherland, S.; Koroleva, O.; Loginov, D. S.; Pecht, I. Intramolecular electron transfer in laccases. *FEB. Journal* **2011**, *278* (18), 3463–3471.
[3]. Reinhammar, B. Optical properties and a new epr signal from type 3 copper in metal-depleted Rhus vernicifera laccase. *J. Inorg. Biochem.* **1983**, *18*, 113–121.
[4]. Le Goff, A.; Holzinger, M.; Cosnier, S. Recent progress in oxygen-reducing laccase biocathodes for enzymatic biofuel cells. *Cell. Mol. Life. Sci.* **2015**, *72* (5), 941–952.
[5]. Cardoso, F.; Aquino Neto, S.; Fenga, P.; Ciancaglini, P.; De andrade, A. Electrochemical characterization of methanol/O2 biofuel cell: Use of laccase biocathode immobilized with polypyrrole film and PAMAM dendrimers. *Electrochimica Acta* **2013**, *90*, 90–94.
[6]. Cardoso, F. P.; Aquino Neto, S.; Crepaldi, L. B.; Nikolaou, S.; Barros, V. P.; De Andrade, A. R. Biocathodes for Enzymatic Biofuel Cells Using Laccase and Different Redox Mediators Entrapped in Polypyrrole Matrix. *J. Electrochem. Soc.* **2014**, *161* (4), F445–F450.
[7]. Parimi, N. S.; Umasankar, Y.; Atanassov, P.; Ramasamy, R. P. Kinetic and Mechanistic Parameters of Laccase Catalyzed Direct Electrochemical Oxygen Reduction Reaction. *ACS. Catal.* **2011**, *2* (1), 38–44.
[8]. Ogikubo, Y.; Akitsu, T. Enhancing Medical or Biological Functions of Laccase by Cyanide-Bridged Cu(II)-Fe(III) Bimetallic Complexes Madiators. *Drug. Des.* **2016**, *5* (2), 130 https://doi.org/10.4172/2169-0138.1000130.
[9]. Kurosawa, Y.; Tsuda, E.; Takase, M.; Yoshida, N.; Takeuchi, Y.; Mitsumoto, Y.; Akitsu, T. Threonine*: Food sources, functions & health benefits,* pp. 73-85; Coleman, J., Ed.; Nova Science: Hauppauge, NY, 2015. ISBN: 978-1-63482-554-2
[10]. *Laccase: Applications, Investigations & Insights*; Harris, A., Ed.; Nova Science: Hauppauge, NY, 2017.
[11]. Savéant, J.; Tard, C. Proton-Coupled Electron Transfer in Azobenzene/Hydrazobenzene Couples with Pendant Acid–Base

Functions. Hydrogen-Bonding and Structural Effects. *J. Am. Chem. Soc.* **2014**, *136* (25), 8907–8910.
[12]. Akitsu, T.; Itoh, T. Polarized spectroscopy of hybrid materials of chiral Schiff base cobalt(II), nickel(II), copper(II), and zinc(II) complexes and photochromic azobenzenes in PMMA films. *Polyhedron* **2010**, *29* (1), 477–487.
[13]. Ito, M.; Akitsu, T.; Palafox, M. A. Theoretical Interpretation of Polarized Light-Induced Supramolecular Orientation on the Basis of Normal Mode Analysis of Azobenzene as Hybrid Materials in PMMA with Chiral Schiff Base Ni(II), Cu(II), and Zn(II) Complexes. *J. Appl. Sol. Chem. Model.* **2016**, *5* (1), 30–47.
[14]. Natansohn, A.; Rochon, P. Photoinduced Motions in Azo-Containing Polymers. *Chem. Rev.* **2002**, *102* (11), 4139–4176.
[15]. Weigert, F. Über einen neuen Effekt der Strahlung. *Naturwissenschaften* **1921**, *9* (30), 583–588.
[16]. Yamazaki, A.; Akitsu, T. Polarized spectroscopy and polarized UV light-induced molecular orientation of chiral diphenyl Schiff base Ni(ii) and Cu(ii) complexes and azobenzene in a PMMA film. *RSC. Adv.* **2012**, *2* (7), 2975.
[17]. Akitsu, T.; Tanaka, R.; Yamazaki, A. Separate observation with polarized electronic and IR spectra of hybrid materials of chiral Mn(II) complexes and azobenzene. *J. Mater. Sci. Eng. A.* **2011**, *1*, 518–525.
[18]. Hariu, N.; Ito, M.; Akitsu, T. Linearly, circularly, or non-polarized light induced supramolecular arrangement of diastereomer Schiff base Ni (II), Cu (II), and Zn (II) complexes by azobenzene in PMMA matrix. *Contemporary Eng. Sci.* **2015**, *8*, 57–70.
[19]. Aritake, Y.; Akitsu, T. The role of chiral dopants in organic/inorganic hybrid materials containing chiral Schiff base Ni(II), Cu(II) and Zn(II) complexes. *Polyhedron* **2012**, *31* (1), 278–284.
[20]. Aritake, Y.; Takanashi, T.; Yamazaki, A.; Akitsu, T. Polarized spectroscopy and hybrid materials of chiral Schiff base Ni(II), Cu(II), Zn(II) complexes with included or separated azo-groups. *Polyhedron* **2011**, *30* (5), 886–894.
[21]. Takase, M.; Akitsu, T. Linearly polarized light-induced anisotropic orientation of binuclear Ni(II), Cu(II), and Zn(II) Schiff base complexes including or without methyl orange in PVA. *Polymer Science Book Series, Volume 1.* Formatex Research Centre, Badajoz, Spain, 2016, 301-308. ISBN: 8494213482.
[22]. Tsuda, E.; Mitsumoto, Y.; Takakura, K.; Sunaga, N.; Akitsu, T.; Konomi, T.; Katoh, M. Electrochemical tuning by polarized UV light induced molecular orientation of chiral salen-type Mn(II) and co(II) complexes in an albumin matrix. *J. Chem. Chem. Eng.* **2016**, 10 53–59.
[23]. Kominato, C.; Akitsu, T. Photoinduced molecular orientation of catalytic-like chiral azo-schiff base complexes in PMMA or laccase matrices, *Letters in Applied NanoBioScience* **2015**, *4*(2), 264-271. https://nanobioletters.com/wp-content/uploads/2021/02/2284680842264270.pdf
[24]. Hayashi, T.; Akitsu, T. *Threonine: Food sources, functions & health benefits*; pp. 49-56, Coleman, J., Ed.; Nova Science: Hauppauge, NY, 2015. ISBN:978-1-63482-554-2
[25]. Ito, M.; Akitsu, T. Polarized UV light induced molecular arrangement depending on flexibility of chiral Schiff Base Ni(II), Cu(II), and Zn(II) complexes by Azobenzene in PMMA matrix. *Contemporary Eng. Sci.* **2014**, *7*, 869–877.
[26]. Hewitt, S. H.; Wilson, A. J. Metal complexes as "protein surface mimetics." *Chem. Commun. (Camb.)* **2016**, *52*, 9745–9756.
[27]. Frisch, M. J.; Trucks, G. W.; Schlegel, H. B.; Scuseria, G. E.; Robb, M. A.; Cheeseman, J. R.; Montgomery, J. A.; Vreven, T.; Kudin, K. N.; Burant, J. C.; Millam, J. M.; Iyengar, S. S.; Tomasi, J.; Barone, V.; Mennucci, B.; Cossi, M.; Scalmani, G.; Rega, N.; Petersson, G. A.; Nakatsuji, H.; Hada, M.; Ehara, M.; Toyota, K.; Fukuda, R.; Hasegawa, J.; Ishida, M.; Nakajima, T.; Honda, Y.; Kitao, O.; Nakai, H.; Klene, M.; Li, X.; Knox, J. E.; Hratchian, H. P.; Cross, J. B.; Adamo, C.; Jaramillo, J.; Gomperts, R.; Stratmann, R. E.; Yazyev, O.; Austin, A. J.; Cammi, R.; Pomelli, C.; Ochterski, J. W.; Ayala, P. Y.; Morokuma, K.; Voth, G. A.; Salvador, P.; Dannenberg, J. J.; Zakrzewski, V. G.; Dapprich, S.; Daniels, A. D.; Strain, M. C.; Farkas, O.; Malick, D. K.; Rabuck, A. D.; Raghavachari, K; Foresman, J. B.; Ortiz, J. V.; Cui, Q.; Baboul, A. G.; Clifford, S.; Cioslowski, J.; Stefanov, B. B.; Liu, G.; Liashenko, A.; Piskorz, P.; Komaromi, I.; Martin, R. L.; Fox, D. J.; Keith, T.; Al-Laham, M. A.; Peng, C. Y.; Nanayakkara, A.; Challacombe, M.; Gill, P. M. W.; Johnson, B.; Chen, W.; Wong, M. W.; Gonzalez, C.; Pople, J. A., Gaussian 09, revision A. 02, Gaussian, Inc., Wallingford CT, 2009.
[28]. Jones, G.; Willett, P.; Glen, R. C.; Leach, A. R.; Taylor, R. Development and validation of a genetic algorithm for flexible docking 1 1Edited by F. E. Cohen. *J. Mol. Bio.* **1997**, *267* (3), 727–748.
[29]. Hewitt, S. H.; Filby, M. H.; Hayes, E.; Kuhn, L. T.; Kalverda, A. P.; Webb, M. E.; Wilson, A. J. Protein surface mimetics: Understanding how ruthenium Tris(bipyridines) interact with proteins. *Chembiochem* **2017**, *18*, 223–231.
[30]. Abu-Dief, A. M.; Mohamed, I. M. A. A review on versatile applications of transition metal complexes incorporating Schiff bases. *Beni-Suef Univ. J. Basic Appl. Sci.* **2015**, *4*, 119–133.
[31]. Abkari, A.; Chaabane, I.; Guidara, K. DFT (B3LYP/LanL2DZ and B3LYP/6311G+(d,p)) comparative vibrational spectroscopic analysis of organic–inorganic compound bis(4-acetylanilinium) tetrachlorocuprate(II). *Physica E: Low-dimensional Systems and Nanostructures* **2016**, *81*, 136–144.
[32]. Ben Gzaiel, M.; Oueslati, A.; Chaabane, I.; Gargouri, M. Density functional theory calculations of the molecular structure and the vibrational spectra of bis-tetrapropyl-ammonium hexachloro-dizincate. *J. Mol. Struc.* **2016**, *1122*, 280–289.
[33]. Zhang, Y.; Du, M.; La, Y.; Yan, Y.; Dong, W. Synthesis, structural characterizations and theoretical calculations of the Ni(II) complex based on a novel Salamo-Salen-Salamo-type hybrid ligand. *J. Mol. Struc.* **2024**, *1296*, 136841.
[34]. Onami, Y.; Kawasaki, T.; Aizawa, H.; Haraguchi, T.; Akitsu, T.; Tsukiyama, K.; Palafox, M. A. Degradation of Human Serum Albumin by Infrared Free Electron Laser Enhanced by Inclusion of a Salen-Type Schiff Base Zn (II) Complex. *Int. J. Mol. Sci.* **2020**, *21* (3), 874, 1–18.
[35]. Sciortino, G.; Rodríguez-Guerra Pedregal, J.; Lledós, A.; Garribba, E.; Maréchal, J. Prediction of the interaction of metallic moieties with proteins: An update for protein-ligand docking techniques. *J. Comput. Chem.* **2017**, *39* (1), 42–51.